Coded Estimation: Design of Backscatter Array Codes for 3D Orientation Estimation

Mohamad Rida Rammal*†, Suhas Diggavi*‡, and Ashutosh Sabharwal§

*Department of Electrical and Computer Engineering, UCLA.

§Department of Electrical and Computer Engineering, Rice University.
Email: †ridarammal@g.ucla.edu, ‡suhasdiggavi@ucla.edu, §ashu@rice.edu

Abstract—We consider the problem of estimating the orientation of a 3D object with the assistance of configurable backscatter tags. We explore the idea of designing tag response codes to improve the accuracy of orientation estimation. To minimize the difference between the true and estimated orientation, we propose two code design criteria. We also derive a lower bound on the worst-case error using Le Cam's method and provide simulation results for multiple scenarios including line-of-sight only and multipath, comparing the theoretical bounds to those achieved by the designs.

Index Terms—Wireless Sensing; RFID tags; Orientation Tracking; Internet-of-Things; Response Design;

I. INTRODUCTION

3D orientation tracking is an important function in many domains, e.g., in robotics, aerospace, and medicine. Orientation can be estimated using many methods, e.g., inertial sensors can be mounted on the object whose orientation has to be measured. Orientation can also be measured using computer vision based methods [1]-[3]. Each of the existing methods have their own pros and cons. For example, inertial sensors may not be suitable for many Internet-of-Things applications, e.g., tracking packages where the solutions have to be very cost-effective. Additionally, the performance of computer vision methods depends on light conditions, and can be difficult for objects that exhibit symmetries.

Wireless sensing has emerged as an interesting alternative sensing modality. Radio-frequency based methods can be useful when visible light wavelengths are not effective, e.g., cases with poor visibility or non-line-of-sight scenarios. In particular, backscatter arrays have been recently used for geolocation and 3D orientation estimation [4], [7]—[9]. Using backscatter arrays is philosophically akin to "painting the faces" of an object, making it a promising option for the orientation detection of symmetric objects such as a solid cube. In this work, we study 3D orientation estimation with the help of configurable backscatter arrays.

In order to aid with the estimation task, one can design the backscatter response to received signals. Specifically, we design the backscatter responses by changing their reflection coefficients. Changing reflection coefficients is possible by switching between different tag load impedances [5], [6]. For example, a tag can switch between two different load

impedances using a multiplexer controlled by a microcontroller (see Fig. 2 in [5]). The design of reflection coefficients can be captured as a binary code specifying what or when the backscatter tags reflect. The problem of finding the best code for the estimation task was first formulated and explored in [10], where we proposed a heuristic code design criterion and had a preliminary exploration of the systems performance.

Related work: In [10], we suggested a heuristic design criteria aimed at maximizing the average-case performance, but did not make attempts to assess its performance. Furthermore, we only considered the average-case error of the system, and did not study the worst-case error, explored in this work. In [8], the authors propose a method for estimating the 3D orientation of an object by measuring the relative phase offset between RFID tags, and aggregating the outputs of multiple 2D estimators. In [9], RFID tags are mounted on carpet pads to measure the 2D orientation of objects in an indoor environment. In [11], a 2D orientation-aware RFID approach is proposed for tracking a target. In [20], the authors track the inclination of objects using UHF RFID tags and a statistical estimator based on the received signal strength. The aforementioned works do not but do not explore the design of backscatter responses and its effect on the estimation problem. In [12], the authors use orthogonal codes (see Section IV for a definition) to distinguish the tags from each other and the environment. [21], [22] use RFID tags to estimate the direction of arrival (DoA). In addition, many other works have considered the use of passive RFID tags for localization and orientation estimation [23]–[26]. However, as far as we know, no past work has considered optimal code design for 3D orientation sensing.

Contributions: In this paper, we revisit the problem and expand our understanding in the following ways. First, we propose two analytic code design criteria that depend on channel knowledge, and investigate their performance with respect to a baseline orthogonal code. We also develop a lower bound on the worst-case error, which quantifies the systems performance with respect to channel parameters such as the number of antennas and the number of tags used. Finally, we provide a comprehensive numerical exploration of the systems performance, including the impact of multipath, and the robustness of the design criteria against imperfect channel

This work is supported in part by NSF grants 1955632, 2146838, 1956297, 2146838.

knowledge. 1

By numerically evaluating the performance, we observe the following. Our design criteria yield codes that offer significant advantages over the channel-oblivious orthogonal code for both the average and worst-case error performance (see Section II-C) for precise definitions). In some cases, our designs provide an order of magnitude improvement in error performance. We also found that *precise* channel knowledge at the transmitter is not critical; Our design criteria are robust against channel estimation errors, retaining almost all improvements when computed with SNR values greater than or equal to 10dB. Furthermore, our numerical results suggest that multipath offers SNR gain but not multipath-diversity gain; this means that when one fixes the total energy received across paths, the performance does not improve when multipath is present.

Organization: Section III describes the channel model and formulates the estimation problem. Section IIII describes the main results, including the two code design criteria. Section IV provides the various numerical results. Finally, Section VI provides proofs for the theorems and lemmas shown in Section IIII.

Notation: \mathbb{R}^k and \mathbb{C}^k are the sets of real-valued and complex-valued k-dimensional vectors, respectively. \mathbf{A}^T and \mathbf{A}^H denote the transpose and conjugate transpose of the matrix \mathbf{A} . If \mathbf{x} is a vector with n elements, then $\mathrm{diag}(\mathbf{x})$ denotes the $n \times n$ square matrix with the elements of \mathbf{x} on its main diagonal; $\|\cdot\|$ is the standard Euclidean norm on vectors, and $\|\cdot\|_F$ is the Frobenius norm on matrices. $\langle\cdot,\cdot\rangle$ is the dot product between two vectors.

II. PROBLEM FORMULATION

A. System Model

We consider an object that can freely rotate around a specific point in space. For ease of computation, we use the 3D coordinate system in which the point the object rotates around is $\mathbf{0} = [0,0,0]^T \in \mathbb{R}^3$. We assume a system having K full-duplex antennas (capable of simultaneously transmitting and receiving in the same frequency band) with position vectors $\boldsymbol{x}_1^{\text{ant}},\ldots,\boldsymbol{x}_K^{\text{ant}} \in \mathbb{R}^3$, and N backscatter tags placed on the object with position vectors $\boldsymbol{x}_1^{\text{tag}},\ldots,\boldsymbol{x}_N^{\text{tag}} \in \mathbb{R}^3$ (see Figure 1).

We specify the orientation of the object using a rotation matrix $Q \in SO(3) \subseteq \mathbb{R}^{3 \times 3}$, where SO(3) is the 3D rotation group. If the object has tags with positions $\boldsymbol{x}_1^{\text{tag}}, \dots, \boldsymbol{x}_N^{\text{tag}}$ on it, and a rotation Q is applied to the object, the tags would have the new positions $Q\boldsymbol{x}_1^{\text{tag}}, \dots, Q\boldsymbol{x}_N^{\text{tag}}$ (see Figure 2). In this framework, we specify the original orientation of the object using the 3×3 identity matrix \boldsymbol{I}_3 .

Each backscatter tag can be configured by setting its state to a value $i \in \{0,1\}$. The state, in turn, determines the reflectivity of the tag. For instance, we may choose to correspond a state of 0 to a reflectivity of +0.5 and a state of 1 to a reflectivity of -0.5. In this scenario, tags reflect regardless of their state. On the other hand, we may choose to correspond a state of 0 to a reflectivity of 0 (does not reflect), and a state of 1 to

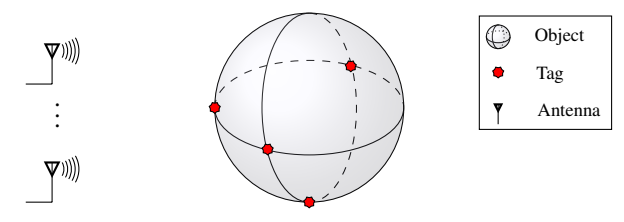


Fig. 1: The components of the considered system. The object along with the tags, rotate around a specific point (in this case, the center of the sphere). The full-duplex antennas interrogate the configurable tags and receive back the reflected signal. We then use the received signal to infer the orientation.

a reflectivity of 1 (reflects) i.e. the state determines the onoff condition of the tag. In addition, the state of each tag can either remain constant (passive) or change over time (active). We study the performance of both options.

The orientation of the object determines the position of the tags, and the states of the tags set their reflectivities. Hence, the orientation and tag states determines the channel model, and in turn the received signal. We use the received signal to estimate the orientation of the object. Our goal is to analyze the performance of this system, and find the best set of tag states for the estimation task. We describe our channel model next

We use the following free-space line-of-sight propagation formula [13] between points $x_1, x_2 \in \mathbb{R}^3$:

$$\eta(\mathbf{x}_1, \mathbf{x}_2) = \frac{1}{4\pi \|\mathbf{x}_1 - \mathbf{x}_2\|} \exp\left(\frac{-2\pi j \|\mathbf{x}_1 - \mathbf{x}_2\|}{\lambda}\right), \quad (1)$$

where λ is the wavelength. In other words, suppose x_{T_x} and x_{R_x} are the position vectors of an isolated transmitter and receiver, and s_{T_x} and s_{R_x} the transmitted and received signals, respectively, then

$$s_{\mathrm{R_x}} = s_{\mathrm{T_x}} \eta(x_{\mathrm{T_x}}, x_{\mathrm{R_x}}). \tag{2}$$

We now specify the matrices involved in our channel model. Let $\boldsymbol{H}_{\boldsymbol{Q}}$ be the $K\times N$ matrix of the line-of-sight responses between the tags and antennas when the object is in orientation \boldsymbol{Q} , i.e. $(\boldsymbol{H}_{\boldsymbol{Q}})_{k,n} = \eta(\boldsymbol{x}_k^{\text{ant}}, \boldsymbol{Q}\boldsymbol{x}_n^{\text{tag}})$. Let \boldsymbol{A} be the symmetric $K\times K$ matrix of inter-antenna line-of-sight responses with $\boldsymbol{A}_{k,k'} = \eta(\boldsymbol{x}_k^{\text{ant}}, \boldsymbol{x}_{k'}^{\text{ant}})$. Let \boldsymbol{B} be the symmetric $N\times N$ matrix of the inter-tag channel responses when the object is in orientation \boldsymbol{Q} . In other words,

$$(\boldsymbol{B}_{\boldsymbol{Q}})_{n,n'} = \eta(\boldsymbol{Q}\boldsymbol{x}_{n}^{\text{tag}}, \boldsymbol{Q}\boldsymbol{x}_{n'}^{\text{tag}}) = \eta(\boldsymbol{x}_{n}^{\text{tag}}, \boldsymbol{x}_{n'}^{\text{tag}}). \tag{3}$$

Applying the same rotation to any two tags does not change the distance between them, so we can drop Q from the subscript of B_Q and use B instead (see Figure 3). Now, let $s_t \in \mathbb{C}^K$ and $s_t' \in \mathbb{C}^N$ be the vectors of the transmitted signals at the antennas and tags respectively at time t, and $\Psi_t \in \mathbb{C}^K$ and $\Psi_t' \in \mathbb{C}^N$ be the vectors of the received signals at the antennas and tags respectively at time t. The relationship between these vectors is given by:

$$\begin{bmatrix} \Psi_t \\ \Psi_t' \end{bmatrix} = \begin{bmatrix} A & H_Q \\ H_Q^T & B \end{bmatrix} \begin{bmatrix} s_t \\ s_t' \end{bmatrix}. \tag{4}$$

¹Note that our method is not necessarily appropriate for real-time orientation estimation in the wild as it requires some calibration.

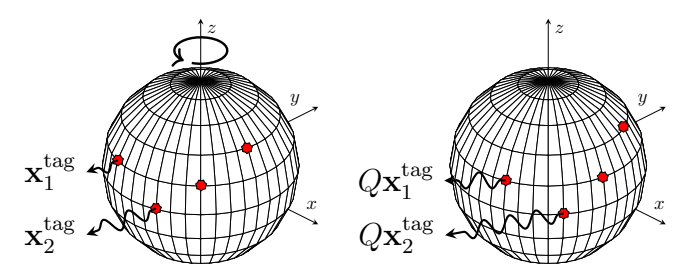


Fig. 2: Rotation of the object about the z-axis. When the object rotates, the tags rotate along with it. The new positions of the tags produce a different received signal. While the tags are equidistant from the point of rotation in the figure, this does not have to be the case.

As we have mentioned before, each backscatter tag can be configured by setting its state to a value $i \in \{0,1\}$, which in turn determines its reflectivity $r_i \in \mathbb{C}$. Hence, the reflectivities can be expressed in terms of the states assigned to the tags. Letting $s_{t,n} \in \{0,1\}$ be the state of the n^{th} tag at time t, $c_t = (s_{t,1}, \ldots, s_{t,N})$ be the codeword at time t (a codeword is a vector of states), and $r(\cdot)$ be the mapping from codewords to reflectivity vectors, we define the matrix of reflectivities at time t as:

$$\mathbf{R}_t = \operatorname{diag}(\mathbf{r}(\mathbf{c}_t)) \in \mathbb{R}^{N \times N}.$$
 (5)

Using the fact that the tags reflect the incident signals, the transmitted signal at the tags is given by $s'_t = R_t \Psi'_t$. We note that the tags also contribute an additive term. A typical RFID reader can easily filter out this component by the receiver's ac-coupling capacitor or DC-offset compensation loop [5] [6]. Thus, we ignore this constant term in our model. Substituting the value of s'_t in [4], and adding the complex Gaussian noise terms $w_t \in \mathbb{C}^K$ and $w'_t \in \mathbb{C}^N$, we obtain the following equations:

$$\Psi_t = As_t + H_O R_t \Psi_t' + w_t \tag{6}$$

$$\mathbf{\Psi}_t' = \mathbf{H}_{\mathbf{O}}^T \mathbf{s}_t + \mathbf{B} \mathbf{R}_t \mathbf{\Psi}_t' + \mathbf{w}_t' \tag{7}$$

Solving the above equations, we obtain that the received signal is given by $\Psi_t = As_t + H_Q R_t (I - BR_t)^{-1} \left(H_Q^T s_t + w_t' \right) + w_t$. We assume that the noise term involving w_t' is dominated by w_t , and hence we ignore the former. Since the first term in the previous expression does not depend on Q, we can subtract it at the receiver yielding a modified noiseless and noisy signals $f(Q; c_t), y(Q; c_t) \in \mathbb{C}^K$ given by:

$$f(Q; c_t) = H_Q R_t (I - BR_t)^{-1} H_Q^T s_t,$$
 (8)

$$y(Q; c_t) = f(Q; c_t) + w_t. \tag{9}$$

B. Codes

The expression in (8) is the *noiseless* channel output when using a codeword c_t . Based on numerical simulations, we have observed that a single codeword often only allows us to detect some orientations, and not others. Specifically, all tag

²We are eliminating full-duplex self-interference, e.g., see [14].

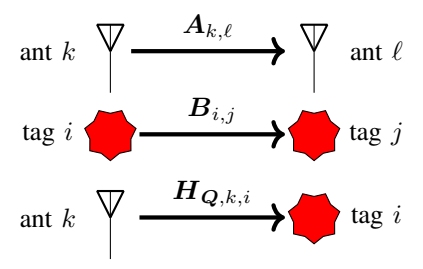


Fig. 3: The matrices associated with the model. For instance, $A_{k,\ell}$ corresponds to the free space loss *from* antennas k to antenna ℓ .

arrays we came across had the following property: for every codeword $c \in \{0,1\}^N$, there exists some Q, Q' such that $Q \neq Q'$ and $f(Q;c) \approx f(Q';c)$ (see Figure 5 in Section IV for such an array). In other words, for every codeword, there is a pair of orientations that the codeword makes almost indistinguishable based on the received signal.

Therefore, using different codewords over time is a natural extension to the model as a new codeword could fill in the gaps left by the ones used previously. Based on this intuition, we define a $code\ C = [c_1 \cdots c_T] \in \{0,1\}^{N \times T}$ to be a binary matrix where each column corresponds to the codeword at a specific time t (See Figure 4). Given the code C, we denote the *concatenated* noiseless and noisy channel outputs as (using F instead of f and f instead of f):

$$F(Q; C) = [f(Q; c_1) \cdots f(Q; c_T)] \in \mathbb{C}^{K \times T}, \quad (10)$$

$$Y(Q; C) = F(Q; C) + W \in \mathbb{C}^{K \times T}, \tag{11}$$

where $W = [w_1 \cdots w_t] \in \mathbb{C}^{K \times T}$ is complex Gaussian noise.

C. Performance Measures

We consider estimation over a finite uniform subset of orientations $\mathcal{Q} \subset \mathrm{SO}(3)$, and use the loss function $\theta(\boldsymbol{Q}, \boldsymbol{Q}')$, equal to the Frobenius norm between the two rotation matrices i.e.,

$$\theta(\mathbf{Q}, \mathbf{Q}') = \|\mathbf{Q} - \mathbf{Q}'\|_{F}. \tag{12}$$

Letting $C \in \{0,1\}^{N \times T}$ be any code, the expected value of the error of C when the ground-truth orientation of the object is $Q \in Q$ is given by:

$$\mathcal{L}(\boldsymbol{Q}, \boldsymbol{C}) = \mathbb{E}_{\boldsymbol{W}} \left[\theta \left(\widehat{\boldsymbol{Q}} \left(\boldsymbol{Y}(\boldsymbol{Q}; \boldsymbol{C}) \right), \boldsymbol{Q} \right) \right]. \tag{13}$$

where $\widehat{Q}(Y(Q;C))$ is the minimum distance decoder to the grid of orientations \mathcal{Q} i.e., the MMSE estimator of Q given Y(Q;C). Assuming a uniform prior over the orientations in \mathcal{Q} ; i.e., the object is equally likely to be in any of the orientations in \mathcal{Q} , the expected value of the error of code C (w.r.t. to the orientations) is given by:

$$\mathcal{L}(C) = \frac{1}{|\mathcal{Q}|} \sum_{Q \in \mathcal{Q}} \mathcal{L}(Q, C), \tag{14}$$

Now, a code that minimizes the average error (w.r.t. to the orientations) could still provide poor performance for a *particular* orientation. In other words, the performance of a code

Time Tag	1	2		Т
1	(((
2	\oints	(• • • •	
:	:	:	٠.	:
N	•	(• • •	(

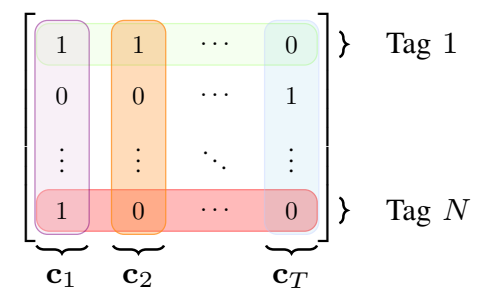


Fig. 4: An illustration of coding over time (left) and its corresponding code (right). Different colors denote different states (reflectivities) of the tag, and different patterns of the states denote different codewords.

C might vary from one orientation to the next. For this reason, we study the worst-case error as it delivers guarantees on the performance across every orientation. We define worst-case error (over all possible orientations in Q) as:

$$\mathcal{M}(C) = \max_{Q \in \mathcal{Q}} \mathcal{L}(Q, C). \tag{15}$$

We believe that both quantities are of interest for designing an orientation estimation system and hence, we suggest criteria for minimizing either depending on the application's particular requirements.

III. THEORETICAL ANALYSIS

Our goal is to find the best code for the estimation task. However, $\mathcal{L}(C)$ in (14) and $\mathcal{M}(C)$ in (15) are intractable. One route we could take is to investigate *tractable* upper or lower bounds on the errors, and minimize those bounds as a proxy for minimizing the errors themselves.

A. Design Criterion For The Average Error

As a proxy for the average error $\mathcal{L}(C)$, we minimize an upper bound to it. We obtain the upper bound on the average error by replacing the probability of misestimating the actual orientation of the object by a tractable quantity. The proof of the following result is given in Section VI-A.

Theorem III.1

Assuming complex white Gaussian noise, the average error $\mathcal{L}(C)$ given in (14) is upper bounded by:

$$\mathcal{U}(C) = \sum_{Q,Q' \in \mathcal{Q}} \operatorname{erfc}\left(\frac{\|F(Q;C) - F(Q';C)\|_F}{2\sqrt{2}\sigma}\right) \theta(Q,Q').$$
(16)

where $\theta(Q, Q')$ is given in [12], erfc is the complement of the Gaussian error function, and σ is the standard deviation of the noise.

Hence, the design criteria for minimizing the average error is simply given by the optimization problem $\min_{\boldsymbol{C}} \mathcal{U}(\boldsymbol{C})$. We can infer the following intuition from $\mathcal{U}(\boldsymbol{C})$ in [16]: good codes should map orientations that are far apart (in terms of θ) to channel outputs that are also far apart. Moreover, since $\operatorname{erfc}(x)$ is tightly upper bounded by $\exp(-x^2)$, $\mathcal{U}(\boldsymbol{C})$ implies that the distance between channel outputs $\|\boldsymbol{F}(\boldsymbol{Q};\boldsymbol{C}) - \boldsymbol{F}(\boldsymbol{Q}';\boldsymbol{C})\|_F$ has an inverse exponential relationship with the average error.

B. Codes For the Worst-Case Error

Whereas we optimize an upper bound for the average error in Section $\boxed{\text{III-A}}$ we obtain a lower bound on the worst-case error $\mathcal{M}(C)$ using Le Cam's method $\boxed{15}$, and minimize the bound to obtain a code for the worst-case performance. The proof of the following theorem is provided in Section $\boxed{\text{VI-B}}$.

Theorem III.2

Assuming complex white Gaussian noise, the worst-case error $\mathcal{M}(C)$ given in (15) is lower bounded by:

$$\mathcal{V}(C) = \max_{Q, Q' \in \mathcal{Q}} \exp\left(-\frac{\left\|F(Q; C) - F(Q'; C)\right\|_F^2}{2\sigma^2}\right) \frac{\theta(Q, Q')}{4},$$
(17)

where $\theta(Q, Q')$ is given in (12).

Hence, the design criteria for minimizing the worst-case error is given by the optimization problem $\min_{C} \mathcal{V}(C)$. $\mathcal{V}(C)$ corroborates the observations from Theorem [III.1] and relates the worst-case error to the model only through the distances between channel outputs. $\mathcal{V}(C)$ again implies that the worst-case error has an inverse exponential relationship with $\|F(Q;C) - F(Q';C)\|_{E}$.

C. Minimax Bound

Unlike Theorem III.2 which suggests a design criteria for the worst-case error using Le Cam's method, the following theorem uses the same tools to quantify the worst-error error decay with parameters including the number of antennas K, the number of tags N through the Frobenius norm of $\boldsymbol{X}^{\text{tag}}$, and the number of samples through the variance σ^2 (as the effective variance of the noise is σ^2/n when provided with n samples). It also reflects the effect of code design on the error.

Theorem III.3 (Minimax Bound)

The worst-case error is bounded as:

$$\mathcal{M}(C) \ge \frac{32\pi^2 \lambda^2 \sigma^2 D^4}{27K^2 \|\boldsymbol{X}^{\text{tag}}\|_F^2 \sum_{t=1}^T \|\widetilde{\boldsymbol{B}}_t\|_F^2 \|\boldsymbol{r}(\boldsymbol{c}_t)\|^2}$$
(18)

where $\widetilde{\boldsymbol{B}}_t = (\boldsymbol{I} - \boldsymbol{B}\boldsymbol{R}_t)^{-1}$ and D is an approximate range between the tagged object and the antennas.

The bound indicates that placing the tags far away from the antennas leads to a larger error. This is clear as the farther away the tags, the weaker the signal we receive due to attenuation. Moreover, it implies an inverse quadratic relationship between the number of antennas and the error. This is again logical because we would be able to receive more power from the reflected signal with more antennas. The bound also reflects the effect of code design through the term $\|\tilde{\boldsymbol{B}}_t\|_F^2 \|\boldsymbol{r}(\boldsymbol{c}_t)\|^2$. For instance, if tags can each have one of two states with corresponding reflectivities 0 and 1 (on or off), then the bound favors most tags to be "on" through the term $\|\boldsymbol{r}(\boldsymbol{c}_t)\|^2$.

D. Structure of the optimal codes

Finding the codes that minimize $\mathcal{U}(C)$ and $\mathcal{V}(C)$ is a combinatorial optimization problem that requires an exhaustive search. Performing an exhaustive search has a running time of $\mathcal{O}(2^{NT})$ if wish to look for the best coding matrix of size T. Hence, for our purposes, finding the best code using bruteforce is intractable except for cases when the number of tags N, and the size of the coding matrix T, are very small.

Therefore, we introduce the idea of code proportions which is essential in reducing the search space. We show that our performance measures depend only on the code through particular proportions of each codeword (see Theorem $\boxed{\text{III.4}}$), therefore reducing the search space to only those proportions. We begin by carefully defining this idea. Let $C = [c_1 \cdots c_T]$ be any code, then we define the proportion of code configuration $c \in \{0,1\}^N$ in C as

$$\pi_c = \frac{1}{T} \sum_{t=1}^{T} 1_{c=c_t}, \tag{19}$$

where $1_{c=c_t}$ is the indicator of the event $\{c=c_t\}$. In other words, π_c is the number of occurrences of c, normalized by T, the size of the code. Moreover, let $c^{(1)},\ldots,c^{(2^N)}$ be an enumeration of the codewords in $\{0,1\}^N$, then we define the vector of code proportions as $\pi=\left[\pi_{c^{(1)}},\cdots,\pi_{c^{(2^N)}}\right]^T$. It is straightforward to see that if two coding matrices share the same size T, and the same proportions vector π , then they are permutations of one another. In what follows, instead of directly using the coding matrix C, we search for the optimal coding scheme through the proportions vector π .

The following theorem allows us to analyze the effect of C on the average and worst-case errors through the proportions vector π . Moreover, we show that the derived bounds in (16) and (17) can be written in terms of π . The proofs of the following results is given in Section VI-F.

Theorem III.4

Assuming independent and identically distributed noise, $\mathcal{L}(C)$ and $\mathcal{M}(C)$ only depend on coding matrix C through the proportions vector π .

Lemma III.1

If we fix T, the size of the code C, then we can write the

minimization of $\mathcal{U}(C)$ and $\mathcal{V}(C)$ in term of π respectively as:

$$\mathcal{U}(\boldsymbol{\pi}) = \sum_{\boldsymbol{Q}, \boldsymbol{Q}' \in \mathcal{Q}} \operatorname{erfc}\left(\sqrt{\frac{T\left\langle\boldsymbol{\pi}, \boldsymbol{g}(\boldsymbol{Q}, \boldsymbol{Q}')\right\rangle}{8\sigma^2}}\right) \theta(\boldsymbol{Q}, \boldsymbol{Q}'), (20)$$

$$V(\boldsymbol{\pi}) = \max_{\boldsymbol{Q}, \boldsymbol{Q}' \in \mathcal{Q}} \exp\left(-\frac{T\left\langle \boldsymbol{\pi}, \boldsymbol{g}(\boldsymbol{Q}, \boldsymbol{Q}')\right\rangle}{2\sigma^2}\right) \theta(\boldsymbol{Q}, \boldsymbol{Q}'), \quad (21)$$

where
$$oldsymbol{g}(oldsymbol{Q},oldsymbol{Q}')\in\mathbb{R}^{2^N}$$
 is given by $oldsymbol{g}(oldsymbol{Q},oldsymbol{Q}')_i=\|oldsymbol{f}(oldsymbol{Q};oldsymbol{c}^{(i)})-oldsymbol{f}(oldsymbol{Q}';oldsymbol{c}^{(i)})\|.$

Theorem III.4 and Lemma III.1 allow us to write our design criteria as optimization problems with respect to the proportions vector π . In (20) and (21), g(Q,Q') represents the link between the design criteria and the channel model. This implies that our design criteria will depend on the channel model only through the distances between channel outputs for different values of the orientation. In other words, the design criteria for the average-case and worst-case errors are respectively given by:

$$\min_{\boldsymbol{\pi} \in \mathbb{R}^{2^{N}}} \quad \sum_{\boldsymbol{Q}, \boldsymbol{Q}' \in \mathcal{Q}} \operatorname{erfc}\left(\sqrt{\frac{T\left\langle\boldsymbol{\pi}, \boldsymbol{g}(\boldsymbol{Q}, \boldsymbol{Q}')\right\rangle}{8\sigma^{2}}}\right) \theta(\boldsymbol{Q}, \boldsymbol{Q}')$$
s.t.
$$\sum_{i=1}^{2^{N}} \boldsymbol{\pi}_{i} = 1, \boldsymbol{\pi} \geq 0.$$
(22)

$$\min_{\boldsymbol{\pi} \in \mathbb{R}^{2^{N}}} \quad \max_{\boldsymbol{Q}, \boldsymbol{Q}' \in \mathcal{Q}} \exp\left(-\frac{T\left\langle \boldsymbol{\pi}, \boldsymbol{g}(\boldsymbol{Q}, \boldsymbol{Q}') \right\rangle}{2\sigma^{2}}\right) \theta(\boldsymbol{Q}, \boldsymbol{Q}')$$
s.t.
$$\sum_{i=1}^{2^{N}} \boldsymbol{\pi}_{i} = 1, \boldsymbol{\pi} \geq 0.$$
(23)

IV. NUMERICAL SIMULATIONS

A. Simulation Setup

We use N=4 backscatter tags that we place randomly within a sphere around the center. The 4 tags can each have two states, with reflection coefficients -0.5 and 0.5, encoded as 0 and 1, respectively. We arrange K=4 full-duplex antennas in a $1m \times 1m$ square on a plane 4m away from the center of the object (see Figure 5 for a sample arrangement). Each antenna emits an identical signal $s_k=1$ for all $k=1,\ldots,K$. We use a wavelength $\lambda=0.005m$, and generate a set of orientations $\mathcal Q$ with $|\mathcal Q|=4096$ by uniformly sampling the ranges of the euler angles and computing the rotation matrices that correspond to the angles.

To find the solution of (22) and (23), we use the well-known trust-region method (TRM) (19). The trust-region method first defines a region around the current solution, and approximates the original objective function using a quadratic model. TRM then takes a step according to what quadratic model depicts in the region. Computing the quadratic approximation to the original objective function grows more computationally demanding as we increase the size Q. However, instead of decreasing the size of Q, we chose to keep Q as is and use a uniform subset of the orientations in Q to solve (22), (23). In particular, for our simulations, we used a set of orientations

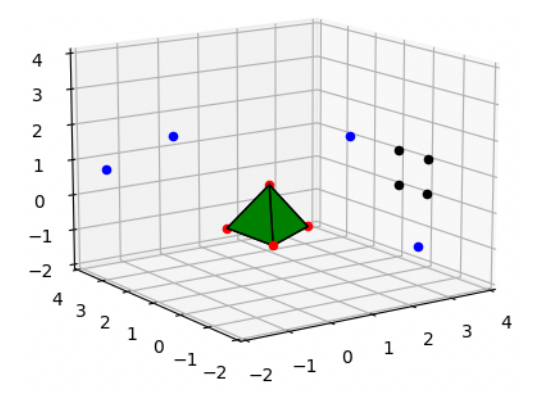


Fig. 5: An example of a simulation setup. The tags (given by the red dots) are in a tetrahedron configuration, while the antennas (given by the black dots) are in a square configuration. Reflectors are denoted by the blue dots.

 $\mathcal{Q}'\subset\mathcal{Q}$ of size 200. The optimization problem requires 5 to 10 minutes to converge on a personal machine. We define SNR as the *received signal-to-noise ratio*, the received signal strength at each antenna, divided by the noise power. In other words $\mathrm{SNR}=10\log_{10}\left(\frac{\|F\|_2^2}{\sigma^2}\right)$, where F is the noiseless signal and σ^2 is the noise variance. We test each value of $\mathrm{SNR}=0,1,\ldots,12$ dB, with trials for each of the 4096 "ground truth" orientations in \mathcal{Q} . As a measure of distance, we use the polar and azimuthal angles in the polar coordinate system (r,θ,φ) . All things considered, the measure of distance we use in our trials is given by:

$$\ell\left[(\theta,\varphi),(\hat{\theta},\hat{\varphi})\right] = (\theta-\hat{\theta})^2 + (\varphi-\hat{\varphi})^2, \tag{24}$$

where (θ,φ) are the ground truth angles, and $(\hat{\theta},\hat{\varphi})$ are the estimated angles. To obtain an estimate $\widehat{\mathcal{L}}(C)$ of the average-case error $\mathcal{L}(C)$, we average the value of the error over the trials, and compute root-mean-square error (RMSE). The performance of a code varies across different orientations. Hence, unique to average error trials, we have included the variance of each coding method at an SNR value of $10 \, \mathrm{dB}$. The variance indicates how much the performance varies from the total average across the different tested orientations. On the other hand, to obtain an estimate $\widehat{\mathcal{M}}(C)$ of the worst-case error $\mathcal{M}(C)$, we average the 500 trials for each of the considered orientations, and then take the maximum over all the orientations in \mathcal{Q} . In these simulation trials, we use codes of size T=24, and compare the performance of the following methods:

- REP_OPT: The best repetition code (all T=24 codewords used are the same). This method is equivalent to the design criteria suggested in [10].
- ORTHOGONAL: The code where each of the vectors in the standard basis $\{e_1, \ldots, e_4\}$ is used 6 times. Note that e_i is the vector components whose are all zero, except for a 1 in the i^{th} component.
- AVERAGE_DESIGN: The method we suggested to minimize the average error. This is the coding scheme that

- minimizes the upper bound of the average error i.e. $\pi^* = \arg\min_{\pi} \mathcal{U}(\pi)$.
- MINIMAX_DESIGN: The method we suggested to minimize the worst-case error. This is the coding scheme that minimizes the lower bound of the worst-case error i.e. $\pi^* = \arg\min_{\pi} \mathcal{V}(\pi)$.

B. The Average and Worst-Case Errors

The results shown in Figure 6 suggest that channel knowledge at the receiver provides significant benefits over orthogonal codes. For the average error, the code we designed, AVERAGE DESIGN, lead to the best performance out of the considered methods, with the code produced by the method we suggested for the worst-case error, MINIMAX DESIGN, trailing behind as a close second. In particular, for the tetrahedron tag configuration shown in Figure 5, the average error when using the code produced by the optimization problem $\min_{\boldsymbol{\pi}} \mathcal{U}(\boldsymbol{\pi})$ is approximately $8 \times$ lower than the error when using orthogonal code. Furthermore, the performance obtained when using the best static code is consistently the worst out of the considered methods. This corroborates the intuition that lead us to introduce the idea of different codes over time. Moreover, the results shown in Figure 6 (bottom) suggest that channel knowledge for code design once again provides benefits for the worst-case error. For the tetrahedron array of Figure 5, the worst-case error produced by the optimization problem $\min_{\boldsymbol{\pi}} \mathcal{V}(\boldsymbol{\pi})$ is approximately $10 \times$ lower than the error produced when using orthogonal codes.

In order to test the effectiveness of the designed criteria on tag arrays different from the one shown in Figure [5], we randomize the positions of the tags (within a sphere of radius 0.25m), compute the designed codes according to the methods of AVERAGE_DESIGN and MINIMAX_DESIGN, and calculate the average and worst-case error ratios obtained when using orthogonal codes versus the designed codes. We perform these steps for a total of 100 times, and produce the density histogram shown in Figure [7]. In many of the 100 trials, the designed codes offered more a significant improvement over the channel oblivious orthogonal code for the average error (Figure [7] top) and worst-case error (Figure [7] bottom).

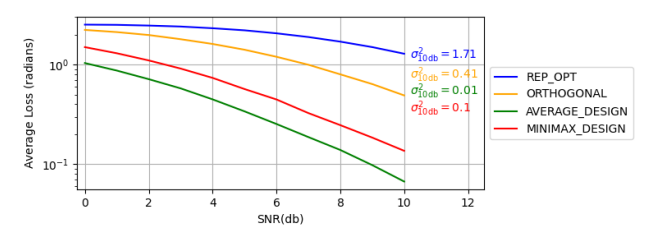
C. Multipath

Suppose we now add M reflectors with positions $\boldsymbol{x}_1^{\mathrm{ref}},\dots,\boldsymbol{x}_M^{\mathrm{ref}}\in\mathbb{R}^3$ to our system. We treat reflectors as virtual sources. For an antenna with position $\boldsymbol{x}_n^{\mathrm{ant}}$, tag with position $\boldsymbol{x}_n^{\mathrm{tag}}$, and reflector with position $\boldsymbol{x}_n^{\mathrm{ref}}$, the ray can take several possible paths: (1) the path that starts at the antenna, passes through the reflector, and ends at the tag, and back the same path, (2) from the antenna to the tag through the LoS path, and then back along the path of the reflector and vice versa. To capture these paths in our model, we define

$$\gamma(\boldsymbol{x}_{k}^{ant}, \boldsymbol{x}_{m}^{\text{ref}}, \boldsymbol{x}_{n}^{tag}) = \eta(\boldsymbol{x}_{k}^{ant}, \boldsymbol{x}_{m}^{\text{ref}}) \eta(\boldsymbol{x}_{m}^{\text{ref}}, \boldsymbol{x}_{n}^{tag}). \tag{25}$$

Let $D_{Q,m}$ be the $K \times N$ matrix of the multipath only channel responses between the tags and antennas in the presence of $\boldsymbol{x}_{m}^{\text{ref}}$, i.e.

$$(\boldsymbol{D}_{\boldsymbol{Q},m})_{k,n} = \gamma(\boldsymbol{x}_k^{\text{ant}}, \boldsymbol{x}_m^{\text{ref}}, \boldsymbol{Q} \boldsymbol{x}_n^{\text{tag}}). \tag{26}$$



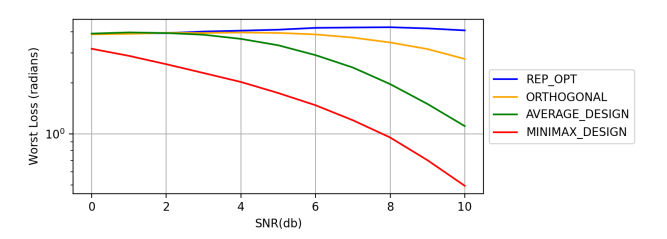
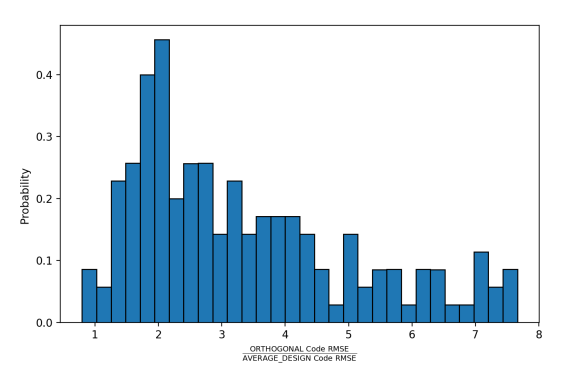


Fig. 6: The average (top) and worst-case (bottom) errors versus SNR for the tag array in Figure 5 At an SNR value of 10dB, the designed code for the average error is nearly $8\times$ more accurate than the channel-agnostic orthogonal code. Meanwhile, the designed code for the worst-case error is nearly $10\times$ more accurate.



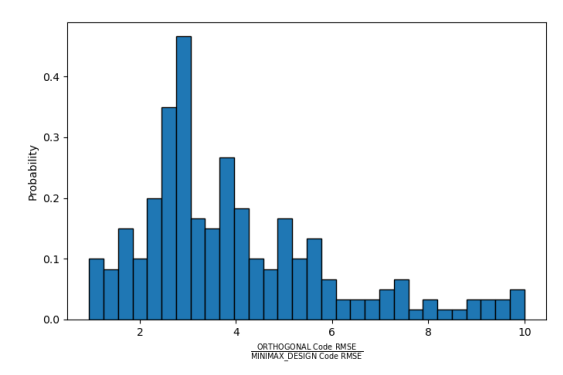


Fig. 7: Probability density histograms for the average error (top) and worst-case error (bottom) ratios when using the orthogonal code and the designed code at an SNR of 10dB.

The matrices involved in our channel model remain largely the same, except for H_Q which is now replaced by $E_Q = H_Q + D_Q$, where $D_Q = \sum_{m=1}^M D_{Q,m}$ The noiseless channel model is thus extended to:

$$\boldsymbol{f}_{m}(\boldsymbol{Q};\boldsymbol{c}_{t}) = \boldsymbol{E}_{\boldsymbol{Q}}\boldsymbol{R}_{t}(\boldsymbol{I} - \boldsymbol{B}\boldsymbol{R}_{t})^{-1}\boldsymbol{E}_{\boldsymbol{Q}}^{T}\boldsymbol{s}_{t}. \tag{27}$$

In our trials, we use 10 multipath components placed 1m away from the object. Based on observations, and the results of Figure 8 multipath does add a small diversity gain. Moreover, given a fixed transmit power, multipath does also offer an SNR gain at the receiver.

D. Robustness

Computing the codes schemes suggested by our design criteria requires channel knowledge. However, we are not likely to have perfect channel knowledge, and so we test the performance of our design criteria when computed using imperfect channel estimation. We introduce channel estimation errors through several methods: (1) adding isotropic noise to channel outputs, (2) adding noise to the inter-tag channel response matrix \boldsymbol{B} , (3) misestimating the reflections coefficients of the tags.

The simplest of introducing channel estimation errors is adding isotropic noise to the channel outputs in different orientations. Specifically, instead of using F(Q;C) to compute the suggested coding scheme, we use

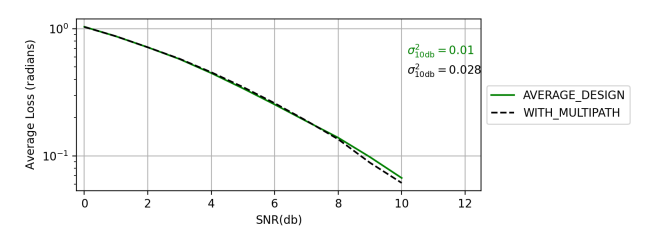
$$F'(Q;C) = F(Q;C) + W_Q, \qquad (28)$$

where W_Q is white Gaussian noise, and W_Q is independent of $W_{Q'}$ for every $Q' \neq Q$. We tested the following values of the SNR = 5, 10, 15dB, with 50 trials each, and then averaged the performance. In particular, the results of Figure 9 indicate that our designed codes retain nearly all even when computed with channel estimation errors greater than or equal to 10dB. The figures also indicate that the design criteria maintain considerable improvement over channel oblivious codes when computed with channel estimation errors less than 10dB.

On the other hand, we can add channel estimation errors by adding noise to the the inter-tag channel response matrix \boldsymbol{B} (see Equation (3)). The noise used is normalized by the entries of \boldsymbol{B} . The results of Figure 10 indicate that misestimating \boldsymbol{B} has a minor effect on the performance when \boldsymbol{B} is misestimated with errors less than or equal to 10dB. Moreover, we add channel errors by misestimating the reflectivity of the tags (e.g. estimating the reflectivity as +0.4, -0.4 when the actual reflectivities are +0.5, -0.5). We measure the misestimation of tag reflection coefficients using the relative absolute error i.e., if we assume true reflectivities 0.5, -0.5 and a relative error of 10%, then we compute the codes under the assumption that the reflectivities are $\{(0.4, -0.4), (0.6, -0.6), (0.4, -0.6), (0.6, -0.4)\}$.

V. CONCLUSION

Active backscatter tags can be very useful when estimating the 3D orientation of objects if tag responses are carefully designed. In this work, we suggested two design criteria, and developed a bound showing how different system parameters



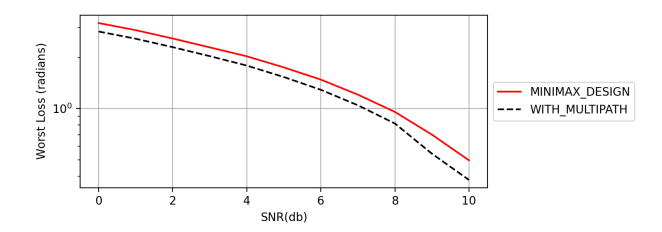
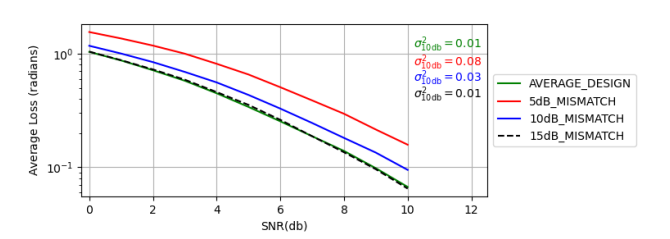


Fig. 8: The average (top) and worst-case (bottom) errors for the designed codes in the cases of line-of-site only and multipath.



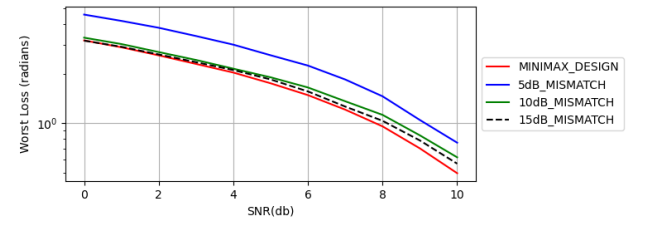


Fig. 9: The average (top) and worst-case (bottom) errors of the designed codes for different levels of channel estimation errors.

affect performance. Through numerical simulations, we exhibited the effectiveness of the suggested designs, and their robustness in the face of imperfect channel knowledge. There are several open questions remaining including designs for more complicated or time-varying environments. Additionally, an exploration of the effectiveness of non-coherent coding in such scenarios is a potentially interesting direction.

VI. PROOFS

A. Proof of Theorem III.1

Let Y = F(Q, C) + W be as in [11]. $\{\widehat{Q}(Y) = Q'\}$ is the event that our estimator outputs a different orientation Q' when the object is in orientation Q. We can rewrite the average error in terms of events of this form.

$$\mathcal{L}(C) = \sum_{Q \in \mathcal{Q}} \mathbb{E}_{W} \left[\theta(\widehat{Q}(Y), Q) \right], \tag{29}$$

$$= \sum_{Q \in \mathcal{Q}} \sum_{Q' \neq Q} \mathbb{P} \left(\widehat{Q}(Y) = Q' \right) \theta(Q, Q'). \tag{30}$$

The probability of the event $\{\widehat{Q}(Y) = Q'\}$ is a difficult quantity to compute outside of cases when $\mathcal Q$ is very small. Therefore, we wish to upper bound it with another probability that is easier to compute. Recall that

$$\widehat{\boldsymbol{Q}}(\boldsymbol{Y}) = \arg\min_{\boldsymbol{Q} \in \mathcal{Q}} \|\boldsymbol{Y} - \boldsymbol{F}(\boldsymbol{Q}, \boldsymbol{C})\|_{F}. \tag{31}$$

Given the functional form of the estimator, a necessary but insufficient condition for our estimator to output Q' is for the received signal Y to satisfy $\|Y - F(Q; C)\| \ge \|Y - F(Q'; C)\|$. Given this relationship between the events, we have that:

$$\left\{ \widehat{\boldsymbol{Q}}(\boldsymbol{Y})\boldsymbol{Q}' \right\} \subseteq \left\{ \left\| \boldsymbol{Y} - \boldsymbol{F}(\boldsymbol{Q}; \boldsymbol{C}) \right\|_{F} \ge \left\| \boldsymbol{Y} - \boldsymbol{F}(\boldsymbol{Q}'; \boldsymbol{C}) \right\|_{F} \right\}.$$
(32)

The latter is event that our *noisy* channel output is closer to the *noiseless* channel output corresponding to Q' than the *noiseless* channel output corresponding to Q. Combining (30)

and (32) with the monotonicity of the probability function $(\mathbb{P}(A) \leq \mathbb{P}(B))$ for all events $A \subseteq B$, we obtain an upper bound on the average error.

$$\mathcal{L}(\boldsymbol{C}) = \sum_{\substack{\boldsymbol{Q} \in \mathcal{Q} \\ \boldsymbol{Q}' \neq \boldsymbol{Q}}} \mathbb{P}\left(\widehat{\boldsymbol{Q}}(\boldsymbol{Y}) = \boldsymbol{Q}'\right) \theta(\boldsymbol{Q}, \boldsymbol{Q}'), \tag{33}$$

$$\leq \sum_{\substack{\boldsymbol{Q} \in \mathcal{Q} \\ \boldsymbol{Q}' \neq \boldsymbol{Q}}} \mathbb{P}\left(\|\boldsymbol{Y} - \boldsymbol{F}(\boldsymbol{Q}; \boldsymbol{C})\|_{F} \geq \|\boldsymbol{Y} - \boldsymbol{F}(\boldsymbol{Q}'; \boldsymbol{C})\|_{F}\right)$$

$$\theta(\boldsymbol{Q}, \boldsymbol{Q}'). \tag{34}$$

In other words, we use the standard pairwise error probability to develop an upper bound to the average error. Combining (34) with the following standard lemma [16], which provides the form for the probability of the event in the right-hand-side of (32), we obtain the desired result.

Lemma VI.1

Let $Y \sim \mathbb{C}\mathcal{N}(\mathbf{0}, \sigma^2 \mathbf{I}_n)$, and let $\mathbf{a} \in \mathbb{C}^n$, then

$$\mathbb{P}(\|\boldsymbol{Y}\| \ge \|\boldsymbol{Y} - \boldsymbol{a}\|) = \frac{1}{2} \operatorname{erfc}\left(\frac{\|\boldsymbol{a}\|}{2\sqrt{2}\sigma}\right), \quad (35)$$

where erfc is the complement of the Gauss error function.

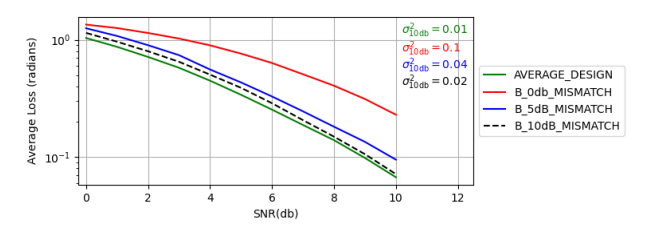
B. Proof of Theorem III.2

Let $C \in [m]^{N \times T}$ be a coding matrix, and let \mathcal{P} be the family of distributions given by

$$\mathcal{P} = \{ \mathbb{C}\mathcal{N}(\mathbf{F}(\mathbf{Q}; \mathbf{C}), \sigma^2 \mathbf{I}); \mathbf{Q} \in \mathcal{Q} \}. \tag{36}$$

The probability distributions in \mathcal{P} can be parameterized by their orientation. Let $P, P' \in \mathcal{P}$ be distributions with Q and Q' as their corresponding orientations, then Le Cam's method [15] asserts that:

$$\mathcal{M}(C) \ge \frac{\theta(Q, Q')}{2} \left(1 - \text{TV}(P, P') \right), \tag{37}$$



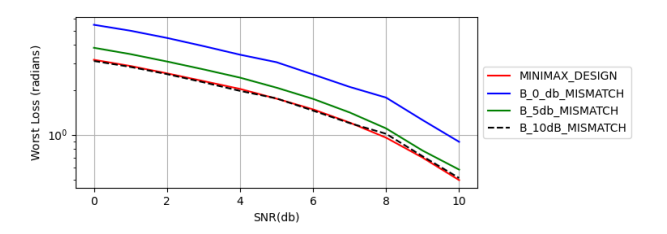
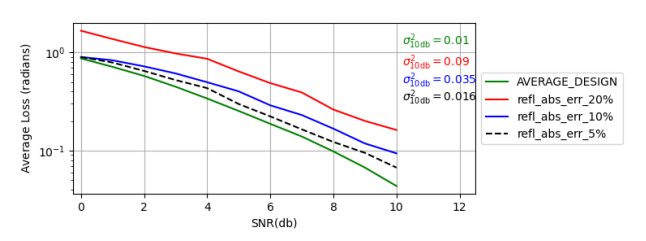


Fig. 10: The average (top) and worst-case (bottom) errors of the designed codes for different levels of channel estimation errors.



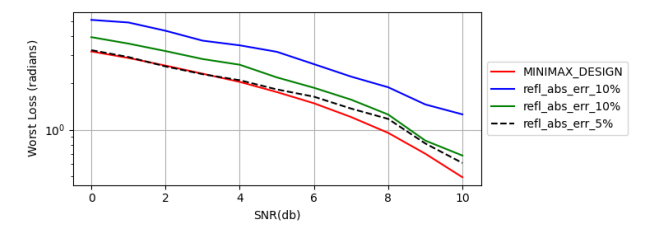


Fig. 11: The average (top) and worst-case (bottom) errors of the designed codes for different levels of channel estimation errors.

where $\mathrm{TV}(P,P')$ is the total variation distance [17]. The Kullback-Leibler divergence [18] is a different and widely used measure of discrepancy between two probability distributions. It has many desirable properties, and it's an upper bound for many other popular discrepancy measures. Through Pinsker's inequality [17], one can upper bound the total-variation distance through the Kullback-Leibler divergence. The total-variation distance between two probability distributions P and P', the Kullback-Leibler divergence, and Pinsker's inequality are respectively given by:

$$TV(P, P') = \int_{\mathbb{C}^{KT}} |P(\boldsymbol{x}) - P'(\boldsymbol{x})| d\boldsymbol{x}.$$
 (38)

$$KL(P||P') = \int_{\mathbb{C}^{KT}} P(\boldsymbol{x}) \log \frac{P(\boldsymbol{x})}{P'(\boldsymbol{x})} d\boldsymbol{x}.$$
 (39)

$$||P - P'||_{\text{TV}} \le \sqrt{\frac{1}{2} \text{KL}(P||P')}.$$
 (40)

$$\mathcal{M}(C) \ge \frac{\theta(Q, Q')}{2} \left(1 - \text{TV}(P, P') \right),$$

$$\ge \frac{\theta(Q, Q')}{2} \left(1 - \sqrt{\frac{1}{2} \text{KL}(P||P')} \right),$$
(41)

$$\geq \frac{\theta(Q, Q')}{4} \exp\left(-\text{KL}(P||P')\right),$$
 (43)

$$=\frac{\theta(\boldsymbol{Q},\boldsymbol{Q}')}{4}\exp\left(-\frac{\left\|\boldsymbol{F}(\boldsymbol{Q};\boldsymbol{C})-\boldsymbol{F}(\boldsymbol{Q}';\boldsymbol{C})\right\|_{F}^{2}}{2\sigma^{2}}\right). \tag{44}$$

(42) follows from Pinsker's inequality, and (43) follows from the inequality $1-x \le e^{-x}$. For two independent Gaussians $P = \mathbb{C}\mathcal{N}(\boldsymbol{\mu}, \sigma^2 \boldsymbol{I})$ and $P' = \mathbb{C}\mathcal{N}(\boldsymbol{\mu}', \sigma^2 \boldsymbol{I})$ with the same co-variance matrix, the Kullback-Leibler divergence is given by $\|\boldsymbol{\mu} - \boldsymbol{\mu}'\|^2 / 2\sigma^2$ [17], and therefore, we obtain (44). Since (44) holds for every $P, P' \in \mathcal{P}$, we can take the maximum

over every pair of distributions (equivalently, every pair of orientations $Q, Q' \in \mathcal{Q}$), which gives

$$\mathcal{M}(C) \ge \max_{\mathbf{Q}, \mathbf{Q}' \in \mathcal{Q}} \exp\left(\frac{-\left\|\mathbf{F}(\mathbf{Q}; \mathbf{C}) - \mathbf{F}(\mathbf{Q}'; \mathbf{C})\right\|_F^2}{2\sigma^2}\right) \frac{\theta(\mathbf{Q}, \mathbf{Q}')}{4}. \quad (45)$$

C. Proof of Theorem III.3

Letting \mathcal{P} be the same family of distributions as in (36), P and P' distributions in \mathcal{P} with Q and Q' as their corresponding distributions, then we can start with Equation (42) which was obtained with Le Cam's method and Pinsker's inequality. In other words, we start with:

$$\mathcal{M}(C) \ge \frac{\theta(Q, Q')}{2} \left(1 - \sqrt{\frac{1}{2} \text{KL}(P||P')} \right),$$
 (46)

where $\mathrm{KL}(P||P')$ is the Kullback-Leibler Divergence. We obtain (46) using Pinsker's inequality [17]. For two independent Gaussians $P = \mathbb{C}\mathcal{N}(\boldsymbol{\mu}, \sigma^2 \boldsymbol{I})$ and $P' = \mathbb{C}\mathcal{N}(\boldsymbol{\mu}', \sigma^2 \boldsymbol{I})$ with the same covariance matrix, $\mathrm{KL}(P, P') = \|\boldsymbol{\mu} - \boldsymbol{\mu}'\|_2 / 2\sigma^2$. Hence,

$$\mathcal{M}(\boldsymbol{C}) \ge \frac{\theta(\boldsymbol{Q}, \boldsymbol{Q}')}{2} \left(1 - \frac{1}{2\sigma} \left\| \boldsymbol{F}(\boldsymbol{Q}; \boldsymbol{C}) - \boldsymbol{F}(\boldsymbol{Q}'; \boldsymbol{C}) \right\|_{F} \right). \tag{47}$$

Now, let R_t be the diagonal matrix of reflectivities when using code configuration c_t , then recall

$$f(Q; c_t) = H_Q R_t (I - BR_t)^{-1} H_Q^T s_t,$$
(48)

$$= \boldsymbol{H}_{\boldsymbol{Q}} (\boldsymbol{I} - \boldsymbol{B} \boldsymbol{R}_t)^{-1} \boldsymbol{R}_t \boldsymbol{H}_{\boldsymbol{Q}}^T \boldsymbol{s}_t, \tag{49}$$

$$= \boldsymbol{H}_{\boldsymbol{Q}} (\boldsymbol{I} - \boldsymbol{B} \boldsymbol{R}_t)^{-1} \operatorname{diag} \left\{ \boldsymbol{H}_{\boldsymbol{Q}}^T \boldsymbol{s}_t \right\} r(\boldsymbol{c}_t), \quad (50)$$

where $r(c_t)$ is the column vector of reflectivities corresponding to code c_t . We wish to bound $||f(Q; c_t) - f(Q'; c_t)||$, so

we use the inequality $\|m{A}_tm{x}_t\| \leq \|m{A}_t\|_F \, \|m{x}_t\|$ with $m{x}_t = m{r}(m{c}_t)$ and

$$egin{aligned} oldsymbol{A}_t = & oldsymbol{H}_{oldsymbol{Q}}(oldsymbol{I} - oldsymbol{B}oldsymbol{R}_t)^{-1} \mathrm{diag}\{oldsymbol{H}_{oldsymbol{Q}'}oldsymbol{s}_t\}. \end{aligned}$$

Lemma VI.2

If D is an approximate range between the tagged object's hinge point and the aperture, then for all $t \in \{1, ..., T\}$

$$\|A_t\|_F \le \left(\frac{K}{4\pi\lambda D^2}\right) \|\boldsymbol{X}^{\text{tag}}\|_F \|\widetilde{\boldsymbol{B}}_t\|_F \theta(\boldsymbol{Q}, \boldsymbol{Q}').$$
 (51)

Letting $\delta = \sqrt{\theta(\boldsymbol{Q}, \boldsymbol{Q}')}$, we have that:

$$\left\| F(Q;C) - F(Q';C) \right\|_{F} \tag{52}$$

$$= \sqrt{\sum_{t=1}^{T} \left\| \boldsymbol{f}(\boldsymbol{Q}; \boldsymbol{c}_{t}) - \boldsymbol{f}(\boldsymbol{Q}'; \boldsymbol{c}_{t}) \right\|}$$
 (53)

$$\leq \sqrt{\sum_{t=1}^{T} \|\boldsymbol{A}_{t}\|_{F}^{2} \|\boldsymbol{r}(\boldsymbol{c}_{t})\|^{2}}$$
 (54)

$$\leq \delta \sqrt{\sum_{t=1}^{T} \underbrace{\left(\frac{K}{2\pi\lambda D^{2}} \left\| \boldsymbol{X}^{\text{tag}} \right\|_{F} \left\| \widetilde{\boldsymbol{B}}_{t} \right\|_{F} \left\| \boldsymbol{r}(\boldsymbol{c}_{t}) \right\| \right)^{2}}_{\Delta_{t}}}, \quad (55)$$

where (54) follows from the inequality $||Ax|| \le ||A||_F ||x||$, and (55) follows from Lemma VI.2 Hence, a lower bound on the worst-case error is given by:

$$\mathcal{M}(C) \ge \frac{\delta^2}{2} \left(1 - \frac{\delta}{2\sigma} \sqrt{\sum_{t=1}^{T} \Delta_t} \right).$$
 (56)

To obtain a tightest bound, we have to find the maximum of the right-hand side with respect to δ . Maximizing (56) with respect to δ is equivalent to finding:

$$\max_{x} \quad x^2 \left(1 - x \right) \tag{57}$$

(57) attains it's maximum value at x = 2/3. This gives us that:

$$\mathcal{M}(C) \ge \frac{32\pi^2 \lambda^2 \sigma^2 D^4}{27K^2 \|\boldsymbol{X}^{\text{tag}}\|_F^2 \sum_{t=1}^T \|\widetilde{\boldsymbol{B}}_t\|_F^2 \|\boldsymbol{r}(\boldsymbol{c}_t)\|_2^2}$$
 (58)

D. Proof of Lemma VI.2

For ease of computation, we drop the t subscript for now, and define $\tilde{B}=(I-BR_t)^{-1}$ with $\tilde{b}_{i,j}=\tilde{B}_{i,j}$, and $\tilde{H}_Q=H_Q\tilde{B}$ with $\tilde{h}_{i,j}^Q=(\tilde{H}_Q)_{i,j}$. Taking $\mathbf{s}_t=\mathbf{1}$, we have that:

$$\|\boldsymbol{A}_{t}\|_{F}^{2} = \sum_{k=1}^{K} \sum_{n=1}^{N} \left| \sum_{i=1}^{K} \tilde{h}_{k,n}^{\boldsymbol{Q}} h_{i,n}^{\boldsymbol{Q}} - \tilde{h}_{k,n}^{\boldsymbol{Q}'} h_{i,n}^{\boldsymbol{Q}'} \right|^{2},$$
 (59)

$$\leq \sum_{k=1}^{K} \sum_{n=1}^{N} \sum_{i=1}^{K} \left| \tilde{h}_{k,n}^{Q} h_{i,n}^{Q} - \tilde{h}_{k,n}^{Q'} h_{i,n}^{Q'} \right|^{2}.$$
 (60)

Using Cauchy-Schwartz inequality, we arrive at:

$$\left\| \tilde{h}_{k,n}^{Q_1} h_{i,n}^{Q_1} - \tilde{h}_{k,n}^{Q_2} h_{i,n}^{Q_2} \right\|^2 \le \left\| \tilde{\mathbf{b}}_n \right\|_2^2 \sum_{l=1}^N \left| h_{k,l}^{Q_1} h_{i,n}^{Q_1} - h_{k,l}^{Q_2} h_{i,n}^{Q_2} \right\|^2$$

Assuming we operate in the far-field region, we can approximate *h* with

$$h_{i,j}^{\mathbf{Q}} = \frac{e^{-j\left(\frac{2\pi}{\lambda}\right)\left\|\mathbf{x}_{i}^{ant} - \mathbf{Q}\mathbf{x}_{j}^{tag}\right\|_{2}}}{4\pi\left\|\mathbf{x}_{i}^{ant} - \mathbf{Q}\mathbf{x}_{j}^{tag}\right\|_{2}} \approx \frac{e^{-j\left(\frac{2\pi}{\lambda}\right)\left\|\mathbf{x}_{i}^{ant} - \mathbf{Q}\mathbf{x}_{j}^{tag}\right\|_{2}}}{4\pi D},$$
(62)

where D is an approximate range between the tagged object's hinge point and the aperture. Hence, we can make the following approximation:

$$\left| h_{k,l}^{\mathbf{Q}} h_{i,n}^{\mathbf{Q}} - h_{k,l}^{\mathbf{Q}'} h_{i,n}^{\mathbf{Q}'} \right|^{2} \approx \left(\frac{1}{4\pi D} \right)^{4} \\
\left| e^{-j\left(\frac{2\pi}{\lambda}\right)} \left(\left\| \mathbf{x}_{k}^{ant} - \mathbf{Q} \mathbf{x}_{l}^{tag} \right\|_{2} + \left\| \mathbf{x}_{i}^{ant} - \mathbf{Q} \mathbf{x}_{n}^{tag} \right\|_{2} \right) \\
- e^{-j\left(\frac{2\pi}{\lambda}\right)} \left(\left\| \mathbf{x}_{k}^{ant} - \mathbf{Q}' \mathbf{x}_{l}^{tag} \right\|_{2} + \left\| \mathbf{x}_{i}^{ant} - \mathbf{Q}' \mathbf{x}_{n}^{tag} \right\|_{2} \right) \right|. \tag{63}$$

Using $1 - e^{-x} \le x$, we can further upper bound (63) by:

$$\left(\frac{\sqrt{\frac{2\pi}{\lambda}}}{4\pi D}\right)^{4} \left(\left\|\mathbf{x}_{k}^{ant} - \boldsymbol{Q}\mathbf{x}_{l}^{tag}\right\|_{2} + \left\|\mathbf{x}_{i}^{ant} - \boldsymbol{Q}\mathbf{x}_{n}^{tag}\right\|_{2} - \left\|\mathbf{x}_{k}^{ant} - \boldsymbol{Q}'\mathbf{x}_{n}^{tag}\right\|_{2} - \left\|\mathbf{x}_{i}^{ant} - \boldsymbol{Q}'\mathbf{x}_{n}^{tag}\right\|_{2}\right).$$
(64)

Using the triangle and matrix norm inequalities in (64), we obtain

$$\left| h_{k,l}^{\boldsymbol{Q}} h_{i,n}^{\boldsymbol{Q}} - h_{k,l}^{\boldsymbol{Q}'} h_{i,n}^{\boldsymbol{Q}'} \right|^{2} \leq 2 \left(\frac{\sqrt{\frac{2\pi}{\lambda}}}{4\pi D} \right)^{4} \left(\left\| \boldsymbol{x}_{l}^{\text{tag}} \right\|_{2}^{2} + \left\| \boldsymbol{x}_{n}^{\text{tag}} \right\|_{2}^{2} \right)$$

$$\theta(\boldsymbol{Q}, \boldsymbol{Q}'). \quad (65)$$

Combining (65) and (60), and summing over the indices of the tags and antennas, we obtain the desired result.

E. Proof of Lemma III.1

Let $C \in \mathbb{R}^{N \times T}$ be a code of size T, and let π be its corresponding proportions vector, then

$$\left\| F(Q;C) - F(Q';C) \right\|_{2}^{2} \tag{66}$$

$$= \sum_{t=1}^{T} \| f(Q; c_t) - f(Q'; c_t) \|_{2}^{2},$$
 (67)

$$= \sum_{t=1}^{T} \sum_{c \in \{0,1\}^{N}} 1_{c_{t}=c} \| f(Q; c) - f(Q'; c) \|,$$
 (68)

$$= \sum_{c \in \{0,1\}^N} \sum_{t=1}^{T} 1_{c_t = c} \| f(Q; c) - f(Q'; c) \|,$$
 (69)

$$=T\sum_{\boldsymbol{c}\in\{0,1\}^{N}}\frac{1}{T}\sum_{t=1}^{T}1_{\boldsymbol{c}_{t}=\boldsymbol{c}}\left\|\boldsymbol{f}(\boldsymbol{Q};\boldsymbol{c})-\boldsymbol{f}(\boldsymbol{Q}';\boldsymbol{c})\right\|,\quad(70)$$

$$= T \sum_{\boldsymbol{c} \in \{0,1\}^N} \boldsymbol{\pi}_{\boldsymbol{c}} \left\| \boldsymbol{f}(\boldsymbol{Q}; \boldsymbol{c}) - \boldsymbol{f}(\boldsymbol{Q}'; \boldsymbol{c}) \right\|, \tag{71}$$

$$=T\left\langle \boldsymbol{\pi},\boldsymbol{g}(\boldsymbol{Q},\boldsymbol{Q}')\right\rangle . \tag{72}$$

Substituting (72) in the expressions of $\mathcal{U}(C)$ and $\mathcal{V}(C)$, we obtain the expressions in (20) and (21).

F. Proof of Theorem III.4

Suppose $C = [c_1 \cdots c_T]$ and $C' = [c'_1 \cdots c'_T]$ are two coding matrices with the same relative weight vectors. In other words, $\pi_c = \pi'_c$ for every code configuration c. If the counts of the different configurations are the same, then there exists some permutation τ on $\{1,\ldots,T\}$ such that $c_{\tau(t)} = c'_t$ for all t. We show the errors do not depend on the ordering of the code configurations due to the iid nature of the noise. To see this, let Y = F(Q; C) + W, then

$$\widehat{Q}(Y) \tag{73}$$

$$=\widehat{Q}\left(F(Q;C)+W\right),\tag{74}$$

$$= \arg\min_{\mathbf{Q}'} \left\| \mathbf{F}(\mathbf{Q}; \mathbf{C}) - \mathbf{F}(\mathbf{Q}'; \mathbf{C}) + \mathbf{W} \right\|_F^2, \tag{75}$$

=
$$\arg\min_{\mathbf{Q}'} \sum_{t=1}^{T} \| f(\mathbf{Q}; c_t) - f(\mathbf{Q}'; c_t) + \mathbf{w}_t \|^2$$
, (76)

$$= \arg\min_{\boldsymbol{Q}'} \sum_{t=1}^{T} \left\| \boldsymbol{f}(\boldsymbol{Q}; \boldsymbol{c}_{\tau(t)}) - \boldsymbol{f}(\boldsymbol{Q}'; \boldsymbol{c}_{\tau(t)}) + \boldsymbol{w}_{\tau(t)} \right\|^{2},$$

$$= \arg\min_{\mathbf{Q}'} \sum_{t=1}^{T} \| f(\mathbf{Q}; c'_t) - f(\mathbf{Q}'; c'_t) + \mathbf{w}_{\tau(t)} \|^2, \quad (78)$$

$$=\widehat{Q}\left(F(Q;C')+W'\right),\tag{79}$$

$$=\widehat{Q}(Y'),\tag{80}$$

where w_t is the $t^{\rm th}$ K-sized block of W, W' is the vector with $w'_t = w_{\tau(t)}$, and Y' = F(Q; C') + W'. Since the elements of W independent and identically distributed, we get that W and W' are also identically distributed. Combining the previous statement with the fact that W and W' are permutations of one another, we can replace any expectation with respect to W with an expectation with respect to W'. Hence,

$$\mathcal{L}(C) = \sum_{Q \in \mathcal{Q}} \mathbb{E}_{W} \left[\theta(\widehat{Q}(Y), Q) \right], \tag{81}$$

$$= \sum_{\boldsymbol{Q} \in \mathcal{Q}} \mathbb{E}_{\boldsymbol{W}} \left[\theta(\widehat{\boldsymbol{Q}}(\boldsymbol{Y}'), \boldsymbol{Q}) \right], \tag{82}$$

$$= \sum_{\boldsymbol{Q} \in \mathcal{Q}} \mathbb{E}_{\boldsymbol{W}'} \left[\theta(\widehat{\boldsymbol{Q}}(\boldsymbol{Y}'), \boldsymbol{Q}) \right], \tag{83}$$

$$=\mathcal{L}(C'). \tag{84}$$

(82) follows from the earlier computation, and (83) follows from the our earlier discussion. Repeating the exact same computation with $\sum_{Q\in\mathcal{Q}}$ replaced with $\max_{Q\in\mathcal{Q}}$ shows that $\mathcal{M}(C)=\mathcal{M}(C')$ i.e. C and C' share the same worst-case performance. Hence, we get that C and C' share the same errors, and that our performance measures depend only on the coding matrix through the relative weight vector. It is worthwhile to note that this property of the errors is not unique to Gaussian noise, but is valid for any noise vector whose components are independent and identically distributed.

REFERENCES

 A. Saxena, J. Driemeyer, and A. Y. Ng, "Learning 3-d object orientation from images," in 2009 IEEE International Conference on Robotics and Automation, pp. 794–800, 2009.

- [2] A. Collet, D. Berenson, S. S. Srinivasa, and D. Ferguson, "Object recognition and full pose registration from a single image for robotic manipulation," in 2009 IEEE International Conference on Robotics and Automation, 2009, pp. 48–55.
- [3] T. Starner, B. Leibe, D. Minnen, T. Westyn, A. Hurst, and J. Weeks, "The perceptive workbench: Computer-vision-based gesture tracking, object tracking, and 3d reconstruction for augmented desks," *Machine Vision and Applications*, vol. 14, pp. 59–71, 2003.
- [4] E. Soltanaghaei, A. Prabhakara, A. Balanuta, M. Anderson, J. M. Rabaey, S. Kumar, and A. Rowe, "Millimetro: Mmwave retro-reflective tags for accurate, long range localization," in *Proceedings of the 27th Annual International Conference on Mobile Computing and Networking*, New York, NY, USA: Association for Computing Machinery, pp. 69–82, 2021.
- [5] C. Boyer, S. Roy, "Backscatter Communication and RFID: Coding, Energy, and MIMO Analysis," in *IEEE Transactions on Communications*, vol. 62, no. 3, pp. 770–785, 2014.
- [6] S. J. Thomas, E. Wheeler, J. Teizer and M. S. Reynolds, "Quadrature Amplitude Modulated Backscatter in Passive and Semipassive UHF RFID Systems," in *IEEE Transactions on Microwave Theory and Techniques*, vol. 60, no. 4, pp. 1175–1182, 2012.
- [7] E. Soltanaghaei, A. Dongare, A. Prabhakara, S. Kumar, A. Rowe, and K. Whitehouse, "Tagfi: Locating ultra-low power wifi tags using unmodified wifi infrastructure," *Proc. ACM Interact. Mob. Wearable Ubiquitous Technol.*, vol. 5, no. 1, pp.1-29, 2021.
- [8] T. Wei and X. Zhang, "Gyro in the air: tracking 3d orientation of batteryless internet-of-things," in *Proceedings of the 22nd Annual International Conference on Mobile Computing and Networking*, pp. 55–68, 2016.
- [9] A. A. N. Shirehjini, A. Yassine, and S. Shirmohammadi, "An rfid-based position and orientation measurement system for mobile objects in intelligent environments," *IEEE Transactions on Instrumentation and Measurement*, vol. 61, no. 6, pp. 1664–1675, 2012.
- [10] K. Chang, N. Raymondi, A. Sabharwal, and S. N. Diggavi, "Wireless paint: Code design for 3D orientation estimation with backscatter arrays," in *IEEE International Symposium on Information Theory, ISIT*, pp. 1224–1229, 2020.
- [11] C. Jiang, Y. He, X. Zheng, and Y. Liu, "Orientation-aware rfid tracking with centimeter-level accuracy," in *Proceedings of the 17th ACM/IEEE International Conference on Information Processing in Sensor Networks*, pp. 290–301, 2018.
- [12] X. Fu, A. Pedross-Engel, D. Arnitz, and M. S. Reynolds, "Simultaneous sensor localization via synthetic aperture radar (sar) imaging," in 2016 IEEE SENSORS, pp. 1–3, 2016.
- [13] D. Tse and P. Viswanath, Fundamentals of Wireless Communication. USA: Cambridge University Press, 2005.
- [14] A. Sabharwal, P. Schniter, D. Guo, D. W. Bliss, S. Rangarajan, and R. Wichman, "In-band full-duplex wireless: Challenges and opportunities," *IEEE Journal on selected areas in communications*, vol. 32, no. 9, pp. 1637–1652, 2014.
- [15] A. N. Shiryayev and Y. A. Koshevnik, "Review: Lucien le cam, asymptotic methods in statistical decision theory," *Bull. Amer. Math. Soc.* (*N.S.*), vol. 20, no. 2, pp. 280–285, 1989.
- [16] U. Madhow, Introduction to Communication Systems, 1st ed. USA: Cambridge University Press, 2014.
- [17] T. M. Cover and J. A. Thomas, Elements of Information Theory (Wiley Series in Telecommunications and Signal Processing). USA: Wiley-Interscience, 2006.
- [18] P. Harremoes and N. Tishby, "The information bottleneck revisited or how to choose a good distortion measure," in 2007 IEEE International Symposium on Information Theory, pp. 566–570, 2007.
- [19] Y. Yuan, "A review of trust region algorithms for optimization," in *Iciam*, vol. 99, no. 1, pp. 271-282. 2000.
- [20] R. Krigslund, P. Popovski and G. F. Pedersen, "Orientation Sensing Using Multiple Passive RFID Tags," in *IEEE Antennas and Wireless Propagation Letters*, vol. 11, pp. 176-179, 2012.
- [21] G. Vougioukas and A. Bletsas, "DoA estimation of a hidden RF source exploiting simple backscatter radio tags," in ICASSP 2021 - 2021 IEEE International Conference on Acoustics, Speech and Signal Processing (ICASSP), pp. 4355-4359, 2021.
- [22] G. Vougioukas and A. Bletsas, "DoA Estimation With a Single Antenna and a Few Low-Cost Backscattering Tags," in *IEEE Transactions on Communications*, vol. 70, pp. 6849-6860, 2022.
- [23] R. -E. -A. Anee and N. C. Karmakar, "Chipless RFID Tag Localization," in *IEEE Transactions on Microwave Theory and Techniques*, vol. 61, pp. 4008-4017, 2013.

- [24] P. Yang, W. Wu, M. Moniri and C. C. Chibelushi, "Efficient Object Localization Using Sparsely Distributed Passive RFID Tags," in *IEEE Transactions on Industrial Electronics*, vol. 60, pp. 5914-5924, 2013.
- [25] W. Zhu, J. Cao, Y. Xu, L. Yang and J. Kong, "Fault-Tolerant RFID Reader Localization Based on Passive RFID Tags," in *IEEE Transactions* on Parallel and Distributed Systems, vol. 25, pp. 2065-2076, 2014.
- [26] M. Scherhäufl, M. Pichler, E. Schimbäck, D. J. Müller, A. Ziroff and A. Stelzer, "Indoor Localization of Passive UHF RFID Tags Based on Phase-of-Arrival Evaluation," in *IEEE Transactions on Microwave Theory and Techniques*, vol. 61, pp. 4724-4729, 2013.



Mohamad Rida Rammal is currently a PhD student at the University of California, Los Angeles. He received his bachelors in Electrical and Computer Engineering and Mathematics from the American University of Beirut (AUB) in 2019, and the M.S. degree in Electrical and Computer Engineering from UCLA in 2021. His research interests include Wireless Imaging, Statistical Learning, and Computer Vision.



Suhas Diggavi is currently a Professor of Electrical and Computer Engineering at UCLA. His undergraduate education is from IIT, Delhi and his PhD is from Stanford University. He has worked as a principal member research staff at AT&T Shannon Laboratories and directed the Laboratory for Information and Communication Systems (LICOS) at EPFL. At UCLA, he directs the Information Theory and Systems Laboratory. His research interests include information theory and its applications to several areas including machine learning, security & privacy,

wireless networks, data compression, cyber-physical systems, bio-informatics and neuroscience; more information can be found at http://licos.ee.ucla.edu

He has received several recognitions for his research from IEEE and ACM, including the 2013 IEEE Information Theory Society & Communications Society Joint Paper Award, the 2021 ACM Conference on Computer and Communications Security (CCS) best paper award, the 2013 ACM International Symposium on Mobile Ad Hoc Networking and Computing (MobiHoc) best paper award, the 2006 IEEE Donald Fink prize paper award among others. He was selected as a Guggenheim fellow in 2021. He also received the 2019 Google Faculty Research Award, 2020 Amazon faculty research award and 2021 Facebook/Meta faculty research award. He served as a IEEE Distinguished Lecturer and also served on board of governors for the IEEE Information theory society (2016-2021). He is a Fellow of the IEEE. He has been an associate editor for IEEE Transactions on Information Theory, ACM/IEEE Transactions on Networking and other journals and special issues, as well as in the program committees of several IEEE conferences. He has also helped organize IEEE and ACM conferences including serving as the Technical Program Co-Chair for 2012 IEEE Information Theory Workshop (ITW), the Technical Program Co-Chair for the 2015 IEEE International Symposium on Information Theory (ISIT) and General co-chair for ACM Mobihoc 2018. He has 8 issued patents.



Ashutosh Sabharwal received the B.Tech. degree from IIT Delhi, New Delhi, India, in 1993, and the M.S. and Ph.D. degrees from The Ohio State University, Columbus, OH, USA, in 1995 and 1999, respectively. He is currently the Department Chair and a Ernest D. Butcher Professor with the Department of Electrical and Computer Engineering, Rice University, Houston, TX, USA. He is the Founder of the WARP Project (warp.rice.edu), an open-source project which is currently in use with more than 125 research groups worldwide and has been used by

more than 500 research articles. He is currently leading several NSF-funded center-scale projects, notably Rice RENEW (renew-wireless.org), to develop an open-source software-defined wireless network platform. His research interests are in wireless theory, design, and large-scale deployed testbeds. He received the 2017 IEEE Jack Neubauer Memorial Award, the 2018 IEEE Advances in Communications Award, the 2019 ACM MobiCom Community Contribution Award, and the 2019 and 2021 ACM Test-of-Time Awards. He is a Fellow of National Academy of Inventors.